

Cyclic behavior of steel beam-concrete wall connections with embedded steel columns (I): Experimental study

Guo-Qiang Li¹, Fulin Gu², Jian Jiang^{*1} and Feifei Sun¹

¹ State Key Laboratory for Disaster Reduction in Civil Engineering, Tongji University, Shanghai 200092, China

² College of Civil Engineering, Tongji University, Shanghai 200092, China

(Received October 05, 2016, Revised December 21, 2016, Accepted January 12, 2017)

Abstract. This paper experimentally studies the cyclic behavior of hybrid connections between steel coupling beams and concrete shear walls with embedded steel columns. Four beam-to-wall connection specimens with short and long embedded steel columns are tested under monotonic and cyclic loads, respectively. The influence of embedment length of columns on the failure mode and performance of connections is investigated. The results show that the length of embedded steel columns has significant effect on the failure mode of connections. A connection with a long embedded column has a better stiffness, load-bearing capacity and ductility than that of a short embedded column. The former fails due to the shear yielding of column web in the joint panel, while failure of the latter is initiated by the yielding of horizontal reinforcement in the wall due to the rigid rotation of the column. It is recommended that embedded steel columns should be placed along the entire height of shear walls to facilitate construction and enhance the ductility.

Keywords: steel coupling beam; beam-to-wall connection; embedded steel column; failure mode; load-bearing capacity

1. Introduction

Reinforced concrete (RC) coupled shear wall systems have been widely used in medium and high-rise buildings where a series of shear walls are connected by coupling beams (ASCE 2010). As the main energy-dissipation component, coupling beams play an important role in the seismic resistance of coupled wall systems. However, traditional RC coupling beams have low ductility and thus limited energy-dissipation capacity, leading to their premature failure under seismic loadings (Pi 2008), as shown in Fig. 1.

Furthermore, it is suggested that the positive longitudinal reinforcement in RC coupling beams should yield before shear failure to satisfy a higher shear capacity demand for seismic designs. This demand leads to a very complex design of coupling beams since they always have a small span-to-depth ratio (i.e., deep beam). Paulay and Binney (1974) proposed a diagonal reinforcement placement in RC coupling beams to enhance their load-bearing and deformation capacity. It was found that the additional diagonal reinforcement resulted in full and stable hysteresis loops, high ductility and good energy dissipation capacity, which significantly enhanced the seismic resistance of shear wall systems (Hindi and Hassan 2004). However, due to the relatively flat slope of the placement of the reinforcement, the diagonal reinforcement contributed less to the shear strength of coupling beams. In addition, longitudinal positive reinforcement was needed at the mid-span to resist

bending moment which complicated the construction of coupling beams. Although the performance of RC coupling beams can be enhanced by adding steel plates (Su and Zhu 2005, Su *et al.* 2009) and using deep beams (Zhao *et al.* 2004), they still suffer from limited ductility and energy dissipation capacity.

To overcome these problems for RC coupling beams, since the 1990s, researchers from America and Canada started to use steel coupling beams with a better shear capacity than RC beams to enhance the ductility of structures (Zhu 2008, Nie *et al.* 2014, Gholhaki and Ghadaksaz 2016). It is desired that steel coupling beams may dissipate more seismic energy given the same stiffness and strength as RC beams. This system is known as hybrid coupled wall (HCW) system. The energy is absorbed as the steel coupling beams undergo inelastic shear deformations and flexural hinges are formed at the bottom of wall piers (Shi *et al.* 2013a). To ensure the energy-absorbing capability of steel coupling beams, a reliable connection between the steel coupling beam and concrete shear wall is essential. The traditional solution is to directly insert the coupling beam into the wall followed by the casting of



Fig. 1 Failure of RC coupling beams (Pi 2008)

*Corresponding author, Ph.D.,
E-mail: jiangjian_0131@163.com

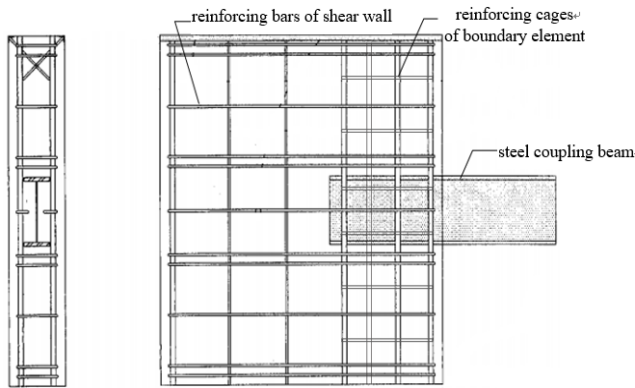


Fig. 2 Traditional connection between embedded steel coupling beam and concrete shear wall (Zhu 2008)

concrete (Shahrooz *et al.* 2004, EI-Tawil *et al.* 2009, Hung and Lu 2015), as shown in Fig. 2. Shahrooz *et al.* (2004) experimentally studied steel beam-wall connections with shear studs on the embedded steel plate. The results showed that the connection was subjected to brittle failure by pulling out of studs. A sufficient embedding length should be guaranteed to ensure the complete load transfer from the coupling beam to the shear wall. Park and Yun (2006a) studied the bearing strength and panel shear strength of connections between structural steel coupling beams and reinforced concrete shear walls. Different layouts of face bearing plates and horizontal ties in the embedded region of the beam were considered. Fortney *et al.* (2007) addressed the superiority of steel coupling beams over RC coupling beams in a shear wall system by carrying out nonlinear analysis of 20-storey shear wall buildings. Recently, Cheng *et al.* (2015) studied the behavior of coupled shear wall systems of steel beams with low yield steel web. The results were compared to the traditional RC coupling beams with diagonal reinforcements. It was found that a ductile behavior of coupled shear wall systems could not be guaranteed by a ductile coupling beam design, and thus the axial and shear strength of RC shear walls should be proportioned based on the provided capacity of coupling beams. Farsi *et al.* (2016) developed replaceable steel coupling beams with end-plate connection which were not embedded into the walls. The experimental results showed a ductile failure with a concentration of inelastic deformation in the steel web which exhibited desirable deformation and energy absorption capacities. Morelli *et al.* (2016) investigated the seismic behavior of two types of coupling beams with beam splice at the middle and end of the beam were considered. It was found that the failure occurred at the beam splice due to the tearing of the web or the bolt hole. Bengar and Aski (2016) compared the seismic behavior of coupled shear wall systems with RC and steel coupling beams. The results showed that the latter had better ductility and energy dissipation capacity. Traditional steel beam-to-wall connections have high stiffness to effectively transfer the shear forces between coupling beam and wall, but have low ductility and suffer from severe strength degradation (ASCE 2010).

To improve the performance of hybrid coupled shear walls and enhance its construction efficiency, a new detail-

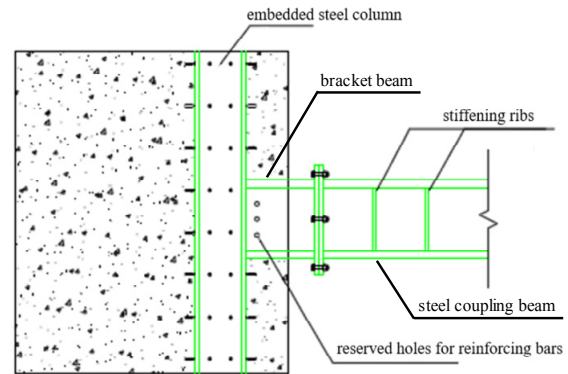


Fig. 3 Schematic of connections between steel coupling beam and concrete shear wall with embedded steel columns

ing of connections between steel coupling beam and concrete shear wall is proposed in this paper, as shown in Fig. 3. A steel bracket, welded to the flange of the imbedded column, projects beyond the face of the concrete shear wall and connects to the steel coupling beam through an extended bolted connection. The coupling beam can thus be replaced due to the presence of brackets, which may facilitate and accelerate the restoration of structures after earthquake. There are rare studies on steel coupling beam-concrete shear wall connection with the embedded steel column. Wu *et al.* (2014a) carried out low cyclic quasi-static loading tests on five steel coupling beam-to-wall connections using bolted end-plate by varying the slenderness ratio of coupling beams. The results showed that the bolted end-plate connection of steel coupling beams had high ductility, good energy dissipation capacity, and insignificant degradation of strength and stiffness.

This paper experimentally investigated the mechanical behavior and failure mode of the connection between steel coupling beams and shear walls by means of embedded steel columns. The influence of the length of embedded steel columns was studied.

2. Test layout

2.1 Design of specimens

The shear deformation governs the behavior of coupling beams and thus there is an inflection point at the mid-span of beams. To simplify the beam-to-wall connection model without changing the boundary conditions, only half of the connection was modeled by applying a concentrated load at the mid-span of beams to simulate the shear force. The shear wall was fixed on the ground with a half-length steel coupling beam connected on the top.

A total of four full-scale specimens were designed and tested with different lengths of embedded steel columns and loading schemes, as listed in Table 1. The lengths of short and long embedded steel columns are 1100 mm and 2900 mm, respectively. Monotonic and low-cyclic loading tests were carried out. The detailed layout of the tested connections with short and long embedded columns is shown in Fig. 4. The hybrid connection can be divided into

Table 1 Parameters of specimens (units: mm)

| No. of specimens | Type of columns | Size of walls (height × thickness × width) | Length of columns | Loading |
|------------------|-----------------|--|-------------------|-----------|
| DJ | Short column | 800×300×3000 | 1100 | monotonic |
| DW | Short column | 800×300×3000 | 1100 | cyclic |
| CJ | Long column | 800×300×2000 | 2900 | monotonic |
| CW | Long column | 800×300×2000 | 2900 | cyclic |

two parts. One is the beam-to-wall part consisting of the embedded steel column, bracket beam, concrete shear wall. The other part is the end-plate bolt connection between the bracket beam and coupling beam, i.e., beam-to-beam part. This beam-to-beam connection may facilitate the replacement of damaged coupling beams after earthquake and can be designed according to relevant codes. This study focuses on the beam-to-wall part.

In this study, the tested concrete shear walls were designed based on Chinese codes (GB 2010, JGJ 2010). The steel columns embedded in the edge of shear walls were designed based on JGJ (2002), and the structural steel members (bracket and coupling beams) were designed based on GB (2003). The steel bracket beam was welded on the flange of the embedded steel column. There were holes prefabricated on the columns and bracket beams to accommodate the arrangement of reinforcement in the shear

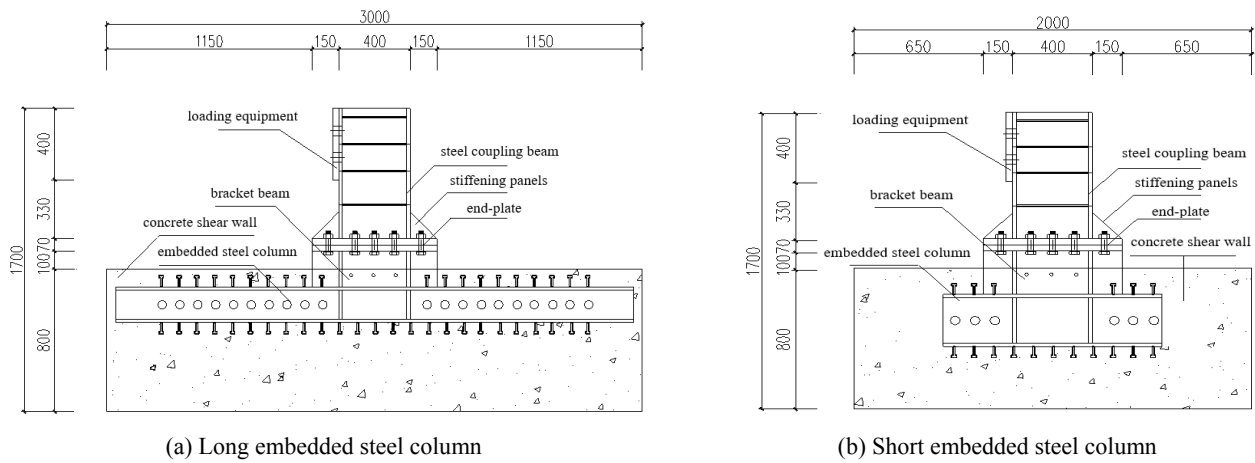


Fig. 4 Layout of the tested connections with short and long embedded columns (all units in mm)

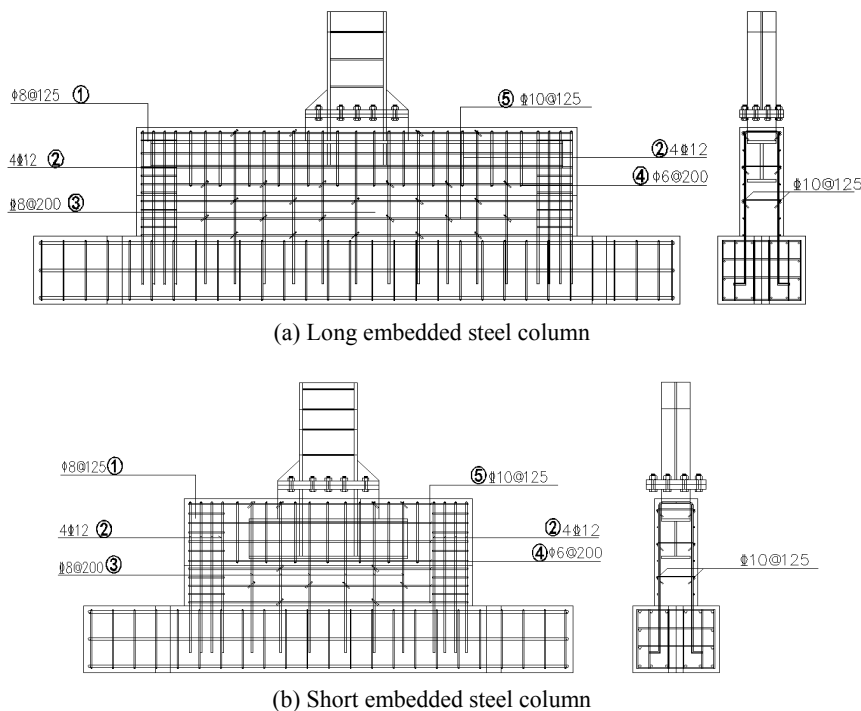


Fig. 5 Layout of reinforcement in the tested connections with short and long embedded columns

Table 2 Parameters of reinforcement in the tested connections

| Type of specimen | Horizontal reinforcement in walls | Vertical reinforcement in walls | Longitudinal reinforcement of embedded column | Stirrups of embedded column | Stirrups of boundary members |
|--------------------|-----------------------------------|---------------------------------|---|-----------------------------|------------------------------|
| Long steel column | $\phi 8@200$ | $\phi 10@125$ | $\phi 12$ | $\phi 8@125$ | $\phi 6@200$ |
| Short steel column | $\phi 8@200$ | $\phi 10@125$ | $\phi 12$ | $\phi 8@125$ | $\phi 6@200$ |

wall. The dimensions of reinforcement and steel members are summarized in Tables 2 and 3, respectively. The arrangement of reinforcement in the shear wall is shown in Fig. 5. Two lines of shear studs were arranged on the flanges of the embedded column, in a longitudinal spacing of 100 mm and transverse spacing of 140 mm. The height and diameter of the studs are 50 mm and 16 mm, respectively. A weak connection was designed and tested in this study to ensure that failure occurred at the connection. The load-transfer mechanism in each component of the connection was studied based on the failure mode observed in the tests, and thus the ultimate capacity of the connection was determined. In practice, the beam-to-wall connection will be over design, according to the predicted strength in this study. This is to ensure that the coupling beam yields first and dissipates more seismic energy, and to guarantee

Table 4 Material properties of steel members

| Steel members | Yielding strength f_y (MPa) | Ultimate strength f_u (Mpa) | Young's modulus E (MPa) |
|---------------|-------------------------------|-------------------------------|---------------------------|
| Beam | 284 | 442 | 2.0×10^5 |
| Column | 329 | 480 | 2.0×10^5 |
| Reinforcement | 557 | 573 | 2.0×10^5 |
| Stirrup | 317 | 535 | 2.0×10^5 |

the concentration of failure on the coupling beam.

The material property of steel was obtained from tensile tests based on GB/T (2010). The yield strength was taken as the stress with a 0.2% offset, and the ultimate strength was taken as the maximum stress in the stress-strain curve. Three coupons were tested and an average value was calculated and adopted in this study, as listed in Table 4. The yield strengths of steel beams, embedded columns, reinforcements, stirrups were 284 MPa, 329 MPa, 557 MPa and 317 MPa, respectively. Their ultimate strengths were 442 MPa, 480 MPa, 573 MPa, 535 MPa, respectively. The Young's modulus of steel was taken as 200 GPa. High strength grade 10.9 friction-grip bolts were used for the beam-to-beam connection. The 28-day compressive strength of concrete was 30.1 MPa.

2.2 Test setup

Fig. 6 shows the test setup. The shear wall was anchored on the reaction floor by 6 bolts in a diameter of 80 mm. The vertical and out-of-plane horizontal movement of the specimen were restrained. The load was imposed by a MTS electrohydraulic servo load testing system with a loading

Table 3 Dimensions of steel members in the tested connections (units: mm)

| Type of specimen | Embedded steel columns | | | | Steel coupling beam | | | |
|-----------------------|------------------------|---------------|--------------|------------------|---------------------|---------------|--------------|------------------|
| | Section height | Web thickness | Flange width | Flange thickness | Section height | Web thickness | Flange width | Flange thickness |
| Long embedded column | 200 | 8 | 200 | 15 | 400 | 16 | 200 | 20 |
| Short embedded column | 300 | 10 | 200 | 15 | 400 | 16 | 200 | 20 |

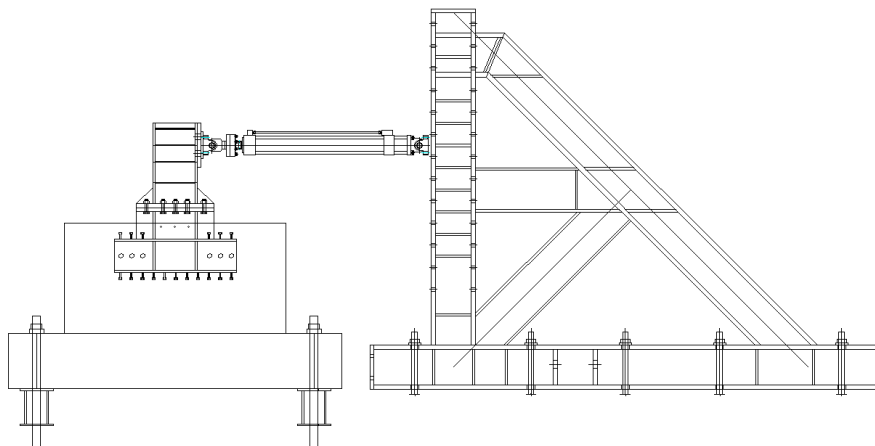


Fig. 6 Test setup

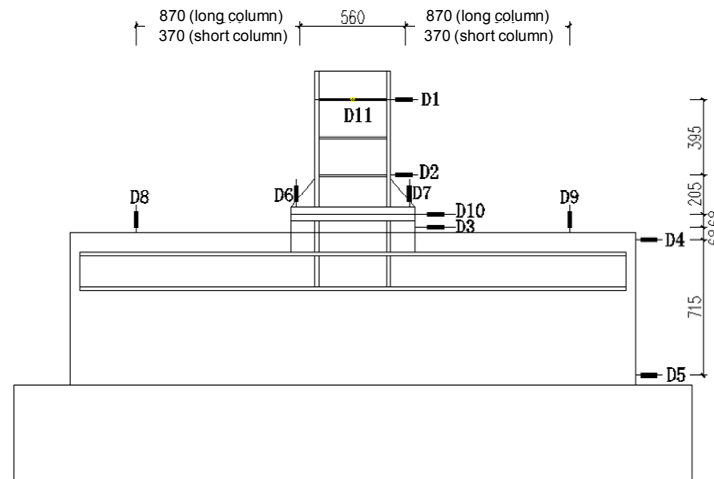


Fig. 7 Layout of displacement LVDTs (all units in mm)

Table 5 Experimental observations of the specimen DJ

| Stage of loading | Test observations |
|--|---|
| Initial stage of loading | Small displacement at the loading point; Initial vertical cracking at the interface of bracket beam flange and concrete |
| $u = 0.6 \text{ mm};$ $\theta = 0.000857 \text{ rad}$ ($P = 50 \text{ kN}$) | Cracking at the interface of embedded steel column flange and concrete |
| $u = 5.0 \text{ mm};$ $\theta = 0.00714 \text{ rad}$ ($P = 420 \text{ kN}$, yielding load) | Load-displacement curve went into nonlinearity with small path of hardening; Long longitudinal cracking at the column-concrete interface; A long plateau in the load-displacement curve |
| $u = 21.0 \text{ mm};$ $\theta = 0.03 \text{ rad}$ ($P = 550 \text{ kN}$, ultimate load) | Beginning of fracture of the longitudinal reinforcement at the outer edge of the embedded column at the tension side of wall |
| $u = 33.0 \text{ mm};$ $\theta = 0.047 \text{ rad}$ | Fracture of all longitudinal reinforcement in the tension side; Load-bearing capacity of the connection reduced dramatically; The reinforcement fractured showed obvious necking |
| Failure | Obvious through crack at the bottom flange of the embedded steel column; Complete separation of the embedded column from the shear wall |

* Note: P = equivalent applied load; u = horizontal displacement at the end of coupling beam (D1); θ = rotation angle of connection

capacity of 2000 kN and displacement range of $\pm 250 \text{ mm}$. The load was applied in the following step:

- (1) The specimens DJ and CJ were tested to failure under monotonic loads by the displacement control. The loading speed was 0.5 mm/min.
- (2) The specimens DW and CW were tested under cyclic loads. In the elastic phase, the loading was

Table 6 Experimental observations of the specimen DW

| Stage of loading | Test observations |
|--|--|
| Loading by force control until 400 kN with interval of $\Delta P = 100 \text{ kN}$ | Initial cracking at the interface of embedded steel column flange and concrete; Similar yielding load and yielding displacement to DJ |
| $u = 5.0 \text{ mm},$ $\theta = 0.00714 \text{ rad}$ | Stiffness degradation (not severe) under cyclic tension load; Stable load-displacement curve under cyclic compression load |
| $u = 20.0 \text{ mm},$ $\theta = 0.0286 \text{ rad}$ | A huge horizontal crack in the shear wall |
| $u = 27.0 \text{ mm},$ $\theta = 0.0386 \text{ rad}$ | Fracture of reinforcement in the tension side; The load-bearing capacity of the connection reduced to 85% of that of DJ |
| $u = 32.0 \text{ mm},$ $\theta = 0.0457 \text{ rad}$ | Loading in one direction until failure; Fracture of most of reinforcement in tension side of the wall; Complete separation of the embedded column from the shear wall; Loss of load-bearing capacity (Fig. 12) |

* Note: P = equivalent applied load; u = horizontal displacement at the end of coupling beam (D1); θ = rotation angle of connection

controlled by forces until the load reached 75% of the ultimate load-bearing capacity obtained from monotonic tests. The displacement-controlled loading was followed in an order of $1.0\delta_y, 1.25\delta_y, 1.50\delta_y, 1.75\delta_y, 2.0\delta_y, 2.5\delta_y, 3.0\delta_y \dots$ (δ_y is the yielding displacement). Three cycles were repeated for each loading step.

The applied loads, vertical and horizontal displacements of specimens, strain of steel members and reinforcement were measured in the test. The imposed load was measured by the force sensor on the loading actuator. The displacements were recorded by linear voltage differential transformers (LVDTs). The arrangement of displacement

Table 7 Experimental observations of the specimen CJ

| Stage of loading | Test observations |
|--|--|
| Initial stage of loading | Similar to DJ |
| $u = 1.0$ mm; $\theta = 0.00143$ rad ($P = 150$ kN) | Initial cracking at the interface of embedded steel column flange and concrete |
| $u = 10.0$ mm; $\theta = 0.0143$ rad ($P = 680$ kN) | Load-displacement curve went into nonlinear with a small path of hardening; Long longitudinal crack at the column-concrete interface; A long plateau in the load-displacement curve |
| $u = 23.0$ mm; $\theta = 0.0329$ rad ($P = 760$ kN) | Beginning of fracture of the longitudinal reinforcement at the outer edge of embedded column at the tension side of wall |
| $u = 42.0$ mm; $\theta = 0.06$ rad | Fracture of most of longitudinal reinforcement in the tension side; Certain level of load-bearing capacity of the connection maintained; |
| $u = 182.0$ mm; $\theta = 0.26$ rad | Tear failure between the flange of embedded steel column and stiffening ribs in the joint area; Load-bearing capacity of the connection reduced dramatically |
| Failure | Large rotation of the connection; Tear of stiffening ribs from the column flange; Loss of load-bearing capacity of the connection; Cracks occurred in the tension side and no crack in the compression side |

* Note: P = equivalent applied load; u = horizontal displacement at the end of coupling beam (D1); θ = rotation angle of connection

measurement points was shown in Fig. 7. The point D1 was to monitor the displacement at the loading point. The points D2~D5 were to measure the relative horizontal displacement where stiffness changed. The relative vertical displacements of the shear wall and endplate were measured by points D6~D10. The D11 was used to record the out-of-plane deformation at the end of coupling beams. The rotation of the coupled connection can then be calculated from the measured vertical and horizontal displacements. Strain gages were attached at the end of steel coupling beam, embedded steel column and reinforcement in the shear wall.

3. Test observations

The experimental observations of the 4 specimens DJ, DW, CJ, CW are summarized in Tables 5-8. The comparison of these four specimens before and after tests is shown in Figs. 8-11. At the failure of the specimen DJ, all the reinforcement at the tension side yielded and its restraining effect on the rotation capacity of the connection reduced. Due to the large bending stiffness, the short

Table 8 Experimental observations of the specimen CW

| Stage of loading | Test observations |
|--|---|
| Loading by force control until 600 kN with interval of $\Delta P = 100$ kN | Initial cracking at the interface of embedded steel column flange and concrete; Similar yielding load and yielding displacement to CJ |
| $u = 10.0$ mm, $\theta = 0.0143$ rad | Stiffness degradation (not severe) under cyclic tension load; Stable load-displacement curve under cyclic compression load |
| $u = 23.0$ mm, $\theta = 0.0329$ rad | Fracture of reinforcement in the tension side; The load-bearing capacity of the connection reduced to 85% of that of CJ |
| Failure | Localized spalling and crushing of concrete in the connection region; Tear of stiffening ribs from the column flange; Fracture of the web of the steel column |

* Note: P = equivalent applied load; u = horizontal displacement at the end of coupling beam (D1); θ = rotation angle of connection



(a) Before the test

(b) After the test

Fig. 8 Behavior of the specimen DJ



(a) Before the test

(b) After the test

Fig. 9 Behavior of the specimen DW

embedded steel column experienced global rigid rotation, leading to an extension of the tension region. The extended tension region resulted in diagonal cracking in the compression region of shear wall (bottom right in Fig. 8(b)) and intense cracking in the tension region (top left in Fig. 8(b)) due to the confining from the reinforcement in the shear wall. Due to the cyclic loading scheme, the distribution of cracks in DW at failure was symmetric. The failure mode of DW was the same as DJ, shown in Fig. 9.

There was obvious necking at the cross-section of reinforcement at the tension side of shear wall CJ at its failure. Due to the small flexure stiffness of long embedded steel column, the column was pulled up by the flange of

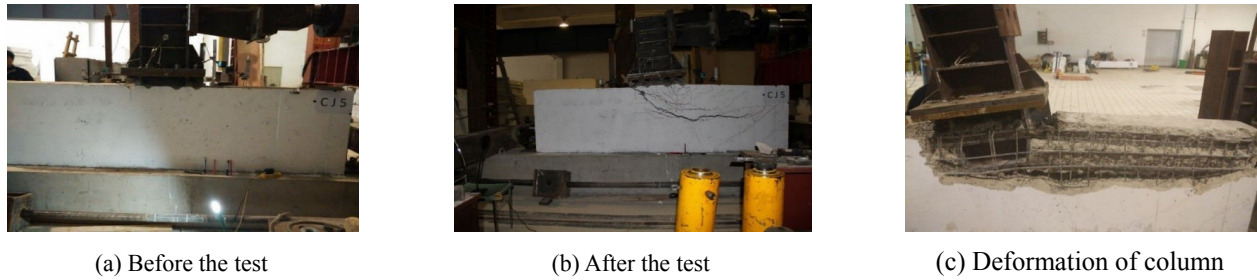


Fig. 10 Behavior of the specimen CJ

bracket beam in the tension side, where the reinforcement first yielded and fractured, as shown in Fig. 10. Taking the advantage of the long anchorage of long embedded steel

column, the load-bearing capacity of CJ was larger than DJ as all the reinforcement in the tension side yielded. The shear strength of the web of the steel column enhanced the load-bearing capacity of the connection. Similarly, a symmetric distribution of cracks was observed in the specimen CW due to the cyclic loading. The web of the embedded steel column fractured because of fatigue. The failure mode of CW was the same as CJ, shown in Fig. 11.

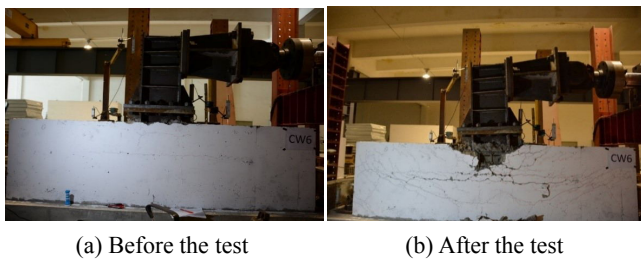


Fig. 11 Behavior of the specimen CW

4. Test measurements

The load-displacement curves for the four specimens DJ, DW, CJ, CW were shown in Fig. 12. For the specimen DJ, the load-displacement curve shows a bilinear variation as shown in Fig. 12(a). After the yielding of the connection,

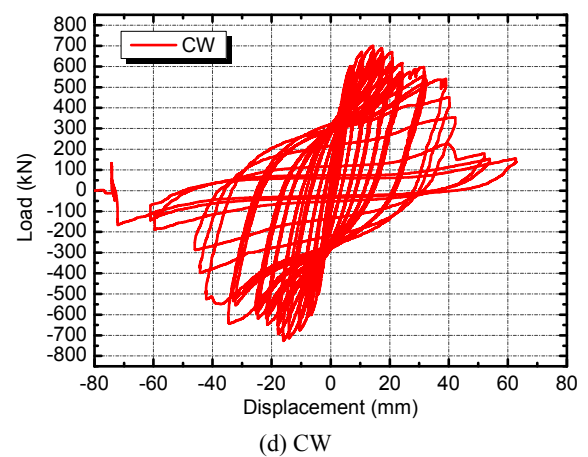
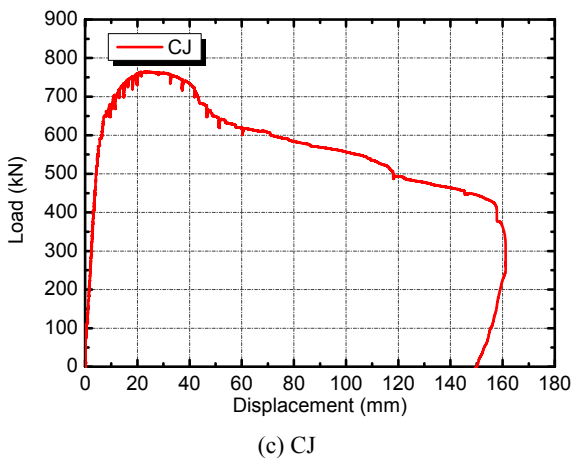
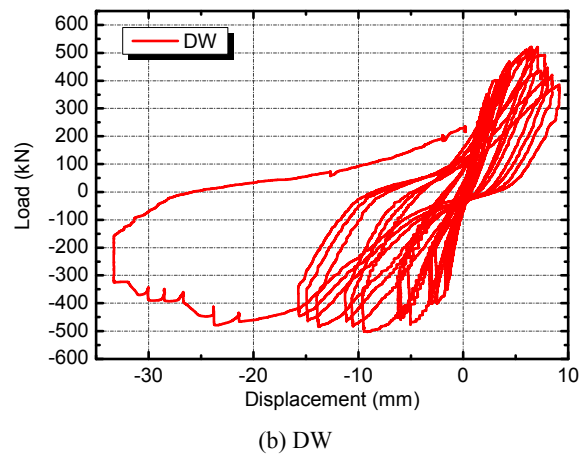
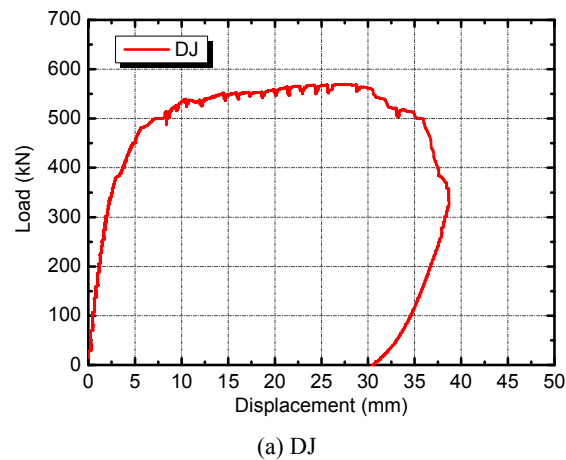


Fig. 12 Load-displacement curves of the specimens

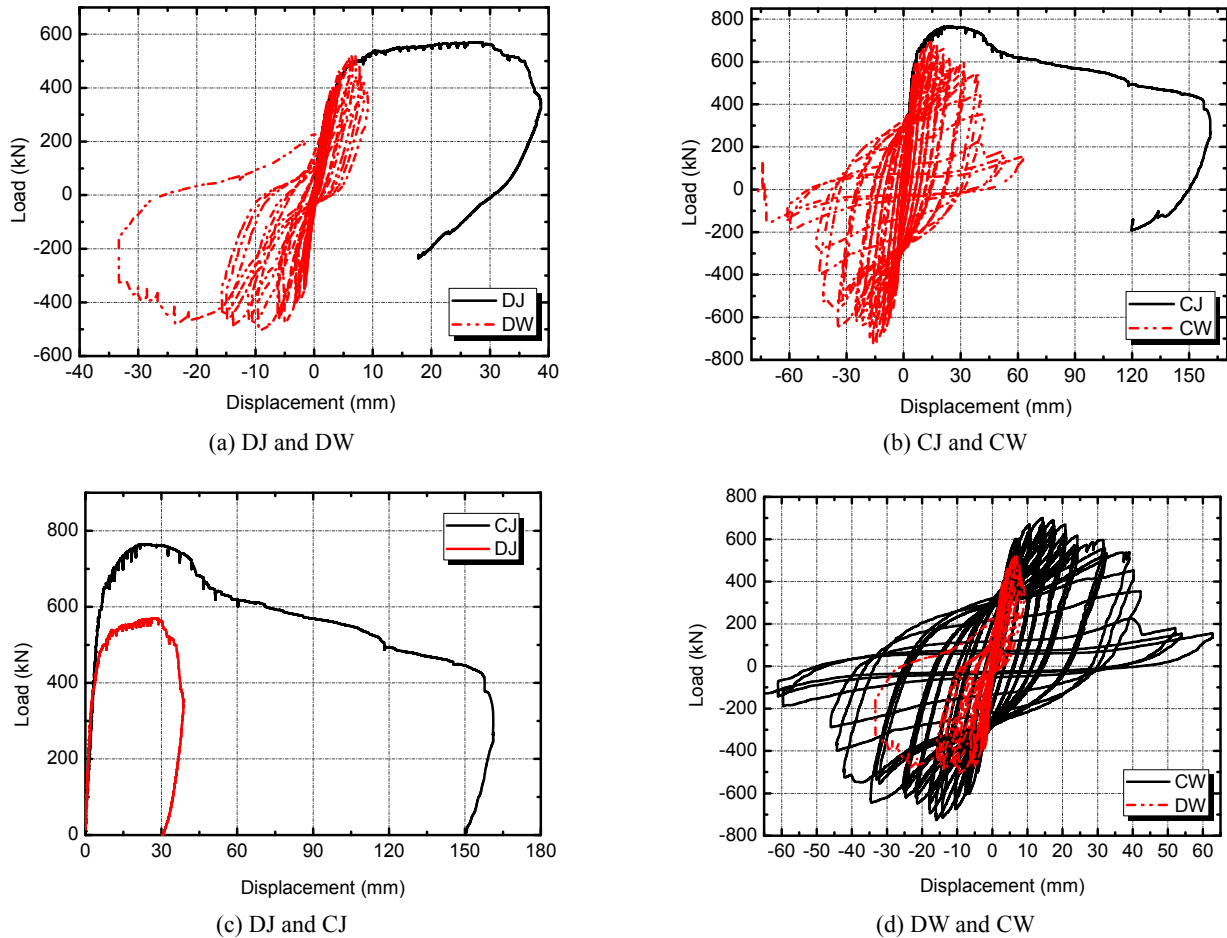


Fig. 13 Comparison of load-displacement curves between the specimens

there was a long plateau without obvious loss of load-bearing capacity. This is because the behavior of the connection with short embedded column is governed by the reinforcement in the shear wall. The load-bearing capacity of the connection reduced dramatically when the reinforcement in tension fractured.

There was obvious pinching effect in the hysteretic response of the specimen DW as shown in Fig. 12(b). This can be attributed to the large residual deformation of reinforcing bars after yielding, the bond failure between reinforcing bars and concrete, and the shear deformation of concrete in the joint region.

The load-displacement curve of the specimen CJ (Fig. 12(c)) shows an inflection point which is due to the shear yielding of web of embedded steel column in the joint zone. The following reduction in load-bearing capacity of connection is because of the fracture of the welding of the stiffening ribs and thus the tear between the column web and flange. Finally, the reinforcement in the shear wall fractured and the load-bearing capacity reduced sharply.

The specimen CW exhibited full and stable loops throughout the test (Fig. 12(d)), due to the energy dissipation from the shear yielding of steel column web.

Fig. 13 shows the comparison of load-displacement curves between DJ and DW, CJ and CW, DJ and CJ, DW and CW. The comparison of monotonic and cyclic loadings of connections with short embedded column (Fig. 13(a))

and long column (Fig. 13(b)) show a good agreement of stiffness for different loading schemes. There was obvious stiffness degradation after yielding for the connection under cyclic loading. The load-bearing capacity from cyclic loading was a bit lower than that from monotonic loading. This is because of accumulated plastic damage under cyclic loading.

The effects of the length of embedded steel columns on the performance of connections under monotonic and cyclic loadings are shown in Figs. 13(c) and (d), respectively. The comparison of load-displacement curves between DJ and CJ (Fig. 13(c)) shows that the connection with a long embedded column had a larger stiffness and load-bearing capacity than that with short column. This is because the longer the anchorage of embedded column, the more reinforcing bars participated, and thus the larger load-bearing capacity of the connection. In addition, the connection with long column had better ductility than that with short column. The comparison of hysteretic loops between DW and CW (Fig. 13(d)) shows that the long column connection achieved more stable and full loops than the short column connection.

The test results are summarized in Table 9. It shows that the connection with a long embedded steel column had larger yielding loads and displacements, larger ultimate loads and displacements, better ductility than that with a short embedded column. The load-bearing capacity of the

Table 9 Summary of test results

| Specimen No. | Yielding load P_y (kN) | Yielding displacement (mm) | Ultimate load P_u (kN) | Ultimate displacement (mm) | Initial stiffness (kN/mm) | Ductility coefficient | P_u/P_y |
|--------------|--------------------------|----------------------------|--------------------------|----------------------------|---------------------------|-----------------------|-----------|
| DJ | 382.2 | 2.5 | 569.3 | 11.11 | 152.88 | 4.44 | 1.49 |
| DW | 350.4 | 2.79 | 521.9 | 6.49 | 125.59 | 2.33 | 1.49 |
| CJ | 554.4 | 3.69 | 765.8 | 23.33 | 150.24 | 6.32 | 1.38 |
| CW | 502.6 | 5.44 | 726.6 | 16.02 | 92.39 | 2.94 | 1.44 |

connection under monotonic loading was larger than that under cyclic loading.

5. Conclusions

This paper experimentally studied the cyclic behavior of hybrid connections between steel coupling beams and concrete shear walls with embedded steel columns. The conclusions may be drawn as follows:

- For a shear wall with embedded steel columns placed through its height (long column), the connection under cyclic loads failed by shear yielding of column web in the joint panel. While the failure of the connection with short embedded columns was caused by the global rotation of the column and thus the yielding of reinforcement.
- The load-bearing capacity of steel beam-to-wall connections can be enhanced by increasing the diameter or decreasing the space of reinforcement, and increasing the shear capacity of steel column web.
- The presence of long embedded column increases the stiffness, load-bearing capacity and ductility of connections, compared to those with short embedded columns.

It is recommended, for practical engineering design, that the embedded steel column should be placed along the entire height of shear walls to not only facilitate the construction process but enhance the ductility of walls. The length of embedded steel columns can be set as the height of storey. The diameter and spacing of stirrups in the joint zone should be increased to enhance the load-bearing capacity of connections.

Acknowledgments

The work presented in this paper was supported the Twelve-Five Science and Technology Support Program with grant 2012BAJ13B02.

References

ASCE (2010), Recommendations for seismic design of hybrid coupled wall systems; Technical Committee on Composite Construction of the Structural Engineering Institute, Reston,

- VA, USA.
- Bengar, H.A. and Aski, R.M. (2016), "Performance based evaluation of RC coupled shear wall system with steel coupling beam", *Steel Compos. Struct., Int. J.*, **20**(2), 337-355.
- Cheng, M.Y., Fikri, R. and Chen, C.C. (2015), "Experimental study of reinforced concrete and hybrid coupled shear wall systems", *Eng. Struct.*, **82**, 214-225.
- El-Tawil S., Fortney, P., Harries, K.A., Shahrooz, B.M., Kurama, Y. and Hassan, M. (2009), "Recommendations for seismic design of hybrid coupled wall systems", *ASCE/SEI*.
- Farsi, A., Keshavarzi, F., Pouladi, P. and Mirghaderi, R. (2016), "Experimental study of replaceable steel coupling beam with end-plate connection", *J. Constr. Steel Res.*, **122**, 138-150.
- Fortney, P.J., Shahrooz, B.M., Gian, A. and Rassati, G.A. (2007), "Seismic performance evaluation of coupled core walls with concrete and steel coupling beams", *Steel Compos. Struct., Int. J.*, **7**(4), 279-301.
- GB (2003), Code for design of steel structures. GB 50017; China Planning Press, Beijing, China.
- GB (2010), Code for design of concrete structures, GB 50010; China Architecture and Building Press, Beijing, China.
- GB/T (2010), Metallic materials—Tensile testing—Part 1: Method of test at room temperature, GB/T 228.1; China Architecture and Building Press, Beijing, China.
- Gholhaki, M. and Ghadaksaz, M.B. (2016), "Investigation of the link beam length of a coupled steel plate shear wall", *Steel Compos. Struct., Int. J.*, **20**(1), 34-41.
- Hindi, R.A. and Hassan, M.A. (2004), "Shear capacity of diagonally reinforced coupling beams", *Eng. Struct.*, **26**(10), 1437-1446.
- Hung, C. and Lu, W. (2015), "Towards achieving the desired seismic performance for hybrid coupled structural walls", *Earthq. Struct.*, **9**(6), 1251-1272.
- JGJ (2002), Technical specification for steel reinforced concrete composite structures; JGJ 138, China Architecture and Building Press, Beijing, China.
- JGJ (2010), Technical specification for concrete structures of tall building; JGJ 3, China Architecture and Building Press, Beijing, China.
- Morelli, F., Manfredi, M. and Salvatore, W. (2016), "An enhanced component based model for steel connection in a hybrid coupled shear wall structure: development, calibration and experimental validation", *Comput. Struct.*, **176**, 50-69.
- Nie, J., Hu, H. and Eatherton, M. (2014), "Concrete filled steel plate composite coupling beams: Experimental study", *J. Constr. Steel Res.*, **94**, 49-63.
- Park, W.S. and Yun, H.D. (2006a), "Seismic performance of steel coupling beam connections in panel shear failure", *J. Constr. Steel Res.*, **62**(10), 1016-1025.
- Park, W.S. and Yun, H.D. (2006b), "Bearing strength of steel coupling beam connections embedded reinforced concrete shear walls", *Eng. Struct.*, **28**(9), 1319-1334.
- Paulay, T. and Binney, J.R. (1974), "Diagonally reinforced coupling beams of shear walls", *International Concrete Abstracts Portal*, **42**, 579-598.
- Pi, T.X. (2008), "Experimental study on seismic behavior and design method study of small span-to-depth ration coupling beams of seismic RC shear walls", Ph.D. Dissertation; Chongqing University, Chongqing, China.
- Shahrooz, B.M., Tunc, G. and Deason, J.T. (2004), "Outrigger beam-Wall connections: Part II—Subassembly testing and further modeling enhancements", *J. Struct. Eng.*, **130**(2), 262-270.
- Shi, Y., Su, M.Z., Mei, X.J. and Jiang, C.Y. (2013a), "Experimental study on hysteretic behavior of innovative hybrid coupled wall system with high coupling ratio", *China Civil Eng. J.*, **46**(1), 52-60.
- Shi, Y., Su, M.Z. and Mei, X.J. (2013b), "Experimental study on

- seismic behavior of hybrid coupled wall system with steel boundary elements”, *J. Earthq. Eng. Eng. Vib.*, **33**(3), 133-139.
- Su, R.K.L. and Zhu, Y. (2005), “Experimental and numerical studies of external steel plate strengthened reinforced concrete coupling beams”, *Eng. Struct.*, **27**(10), 1537-1550.
- Su, R.K.L., Lam, W.Y. and Pam, H.J. (2009), “Experimental study of plate reinforced composite deep coupling beams”, *Struct. Des. Tall Special Build.*, **18**(3), 235-257.
- Wu, Y.T., Dai, C.M. and Xiao, Y. (2014a), “Seismic performance of bolted endplate steel coupling beams for coupled composite shear wall”, *China Civil Eng. J.*, **12**(5), 39-48.
- Wu, Y.T., Dai, C.M. and Zhou, Z.L. (2014b), “Seismic behavior of shear dominant bolted endplate steel coupling beam of composite coupled shear wall”, *J. Build. Struct.*, **35**(4), 255-261.
- Zhao, Z.Z., Kwan, A.K.H. and He, X.G. (2004), “Nonlinear finite element analysis of deep reinforced concrete coupling beams”, *Eng. Struct.*, **26**(1), 13-25.
- Zhu, H. (2008), “Experimental study and analysis on bearing capacity of connection between steel coupling beam and concrete shear wall”, Ph.D. Dissertation; Central South University, Changsha, China.